ACS APPLIED MATERIALS & INTERFACES

Research Article

www.acsami.org

Sea-Urchin-Like Au Nanocluster with Surface-Enhanced Raman Scattering in Detecting Epidermal Growth Factor Receptor (EGFR) Mutation Status of Malignant Pleural Effusion

Lei Wang,[†,∇] Ting Guo,[‡,∇] Qiang Lu,[†,∇] Xiaolong Yan,[†] Daixing Zhong,[†] Zhipei Zhang,[†] Yunfeng Ni,[†] Yong Han,[†] Daxiang Cui,*[,§] Xiaofei Li,*[,†] and Lijun Huang*[,†]

[†]Department of Thoracic Surgery, Tangdu Hospital, The Fourth Military Medical University, Xi'an, Shaanxi 710038, China

[‡]Department of Pain Management, Tangdu Hospital, The Fourth Military Medical University, Xi'an, Shaanxi 710038, China

[§]Department of Bio-Nano-Science and Engineering, National Key Laboratory of Nano/Micro Fabrication Technology, Key Laboratory for Thin Film and Microfabrication of Ministry of Education, Institute of Micro-Nano Science and Technology, Shanghai Jiao Tong University, Shanghai, 200240, China

Supporting Information

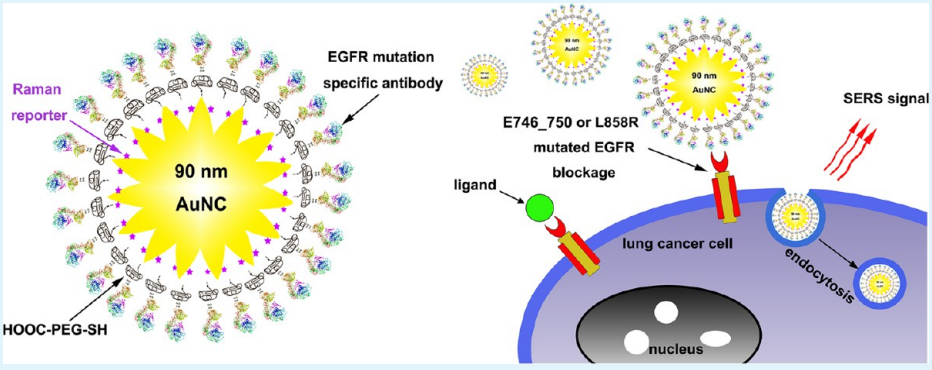

ABSTRACT: Somatic mutations in the epidermal growth factor receptor (EGFR) gene are common in patients with lung adenocarcinomas and are associated with sensitivity to the small-molecule tyrosine kinase inhibitors (TKIs). For 10%−50% of the patients who experienced malignant pleural effusion (MPE), pathological diagnosis might rely exclusively on finding lung cancer cells in the MPE. Current methods based on polymerase chain reaction were utilized to test EGFR mutation status of MPE samples, but the accuracy of the test data was very low, resulting in many patients losing the chance of TKIs treatment. Herein, we synthesized the sea-urchin-like Au nanocluster (AuNC) with an average diameter of 92.4 nm, composed of 15-nm nanopricks. By introducing abundant sharp nanopricks, the enhancement factor of AuNC reached at 1.97×10^7. After capped with crystal violet (CV), polyethylene glycol, and EGFR mutation specific antibody, the AuNC-EGFR had excellent surface-enhanced Raman scattering (SERS) activity and EGFR mutation targeted recognition capability in lung cancer cells. Characteristic SERS signal at 1617 cm^{-1} of CV was linear correlation with the number of H1650 cells, demonstrating the minimum detection limit as 25 cells in a 1-mL suspension. The gold mass in single H1650 cells exposed to AuNC-E746_750 for 2 h ranged from 208.6 pg to 231.4 pg, which approximately corresponded to 56−62 AuNCs per cell. Furthermore, SERS was preclinically utilized to test EGFR mutation status in MPE samples from 35 patients with lung adenocarcinoma. Principal component analysis (PCA) and the support vector machine (SVM) algorithm were constructed for EGFR mutation diagnostic analysis, yielding an overall accuracy of 90.7%. SERS measurement based on sea-urchin-like AuNC was an efficient method for EGFR mutation detection in MPE, and it might show great potential in applications such as predicting gene typing of clinical lung cancer in the near future.

KEYWORDS: *epidermal growth factor receptor, lung cancer, sea-urchin-like Au nanoclusters, surface-enhanced Raman scattering, malignant pleural effusion*

1. INTRODUCTION

Lung cancer is the leading cause of cancer death in the world, with a five-year survival rate of 15%.[1] Non-small-cell lung cancer (NSCLC) accounts for 80% of the lung cancer and is further categorized into specific subtypes: adenocarcinoma, squamous cell carcinoma, large cell carcinoma, and so on.[2] The epidermal growth factor receptor (EGFR) is a member of the receptor tyrosine kinase family, which is included in the erbB

Received: September 15, 2014
Accepted: December 15, 2014
Published: December 15, 2014

DOI: 10.1021/am508122e
ACS Appl. Mater. Interfaces 2015, 7, 359−369

family. Somatic mutations in the EGFR gene are detectable in 50% of Asian patients with lung adenocarcinoma and are associated with sensitivity to small-molecule tyrosine kinase inhibitors (TKIs).[3,4] The patients only with EGFR mutation can win an improved progression-free survival and overall survival with TKIs.[4] The most commonly lung cancer-associated EGFR mutations are deletions in exon 19 (E746_750) and the point mutation in exon 21 (L858R), accounting for ∼85%−90% of total mutation.[3−5]

Direct DNA sequencing of polymerase chain reaction (PCR)-amplified genomic DNA fragments of cancerous tissues is the preferred method for optimal EGFR mutation detection.[5,6] However, only <30% patients are eligible for surgical resection as advanced staging excludes the surgical approach, thus limiting the availability of cancerous tissues for EGFR mutation analysis.[7] Between 10% and 50% of the patients experience malignant pleural effusion (MPE), for whom pathological diagnosis may rely exclusively on finding lung cancer cells in the MPE.[8] Many methods based on PCR are currently utilized to test the EGFR mutation status of MPE samples, but the accuracy of data is very low, leading to many patients losing the chance of having TKIs treatment.[9,10] Because of the paucity of cancer cells and/or large cellular heterogeneity, highly sensitive mutation detection methods are highly desirable for MPE samples.[7]

Surface-enhanced Raman scattering (SERS) offers great promise for simplified, sensitive detection of biomolecular interactions and several advantages in early diagnosis over the previously mentioned assay methodologies.[11,12] Gold nanoparticles covered by Raman reporters and antibodies have been used for SERS to detect cancer cells *in vitro* and tumors *in vivo*.[13−16] The biocompatible gold nanoparticles could produce an optical contrast to distinguish cancer from normal cells.[16] In our team, 90-nm gold nanoparticles were previously capped by a Raman reporter, and an EGFR specific antibody-drug (Cetuximab), and these drug/SERS gold nanoparticles presented a high SERS signal both in cancer cells and in mice bearing xenograft tumors.[17] Moreover, extensive tumor growth inhibition in mice could be simultaneously observed through the evaluation of Raman signal.[17] SERS detection shows the excellent potential for trace cell detection; nevertheless, the use of SERS nanoparticles as a diagnostic tool to detect EGFR mutation status in MPE sample has never been reported previously.

In previous research, we synthesized sea-urchin-like Au nanoclusters (AuNC) and Au microspheres, which possessed excellent SERS activity for the detection of biomolecules.[18−20] This sea-urchin-like AuNC with abundant nanobridges, sharp protrusions, or crevices has obtained a high SERS activity and an improved uniformity and reproducibility of SERS signal.[21,22] Herein, in order to maximize the sensitivity, uniformity, biocompatibility, and reproducibility of the SERS signal, we improved the synthetic process and acquired sea-urchin-like AuNC with more nanopricks and smaller size. By introducing abundant sharp nanopricks, the enhancement factor (EF) of single AuNC was improved to 1.97×10^7, winning an improved uniformity and reproducibility of SERS signal. The small-sized nanoclusters were in favor of the process of endocytosis by cells, and an improved biocompatibility has been obtained. After being capped with a Raman reporter (crystal violet, CV), EGFR mutation-specific antibodies, and polyethylene glycol (PEG), this antibody/SERS AuNC exhibited more-favorable SERS activity and biocompatibility, and were utilized for EGFR mutation analysis in lung cancer cells and clinical MPE samples.

2. EXPERIMENTAL SECTION

2.1. Reagents and Materials. All chemicals ($HAuCl_4 \cdot 3H_2O$, ascorbic acid (AA), and sodium citrate) were purchased from Sigma−Aldrich (USA) Chemical Reagent Co. Ultrapure water (18.4 MΩ cm^{-1}) was prepared using a Millipore Milli-Q system and used throughout the work. The following chemicals were obtained from commercial sources and were used without further purification: CV dye (Sigma−Aldrich, USA), mPEG-SH (MW ≈ 5000 Da) (JenKem Technology Co, Beijing, China), HS-PEG-COOH (MW ≈ 5000 Da) (JenKem Technology Co, Beijing, China), EGFR E746_750 mutation-specific monoclone antibody (rabbit IgG, Catalog No. 2085, Cell Signaling Technologies, Danvers, MA), EGFR L858R mutation specific monoclone antibody (rabbit IgG, Catalog No. 3197, Cell Signaling Technologies, Danvers, MA). All other reagents were obtained from Sigma−Aldrich (St. Louis, MO) at the highest purity available.

2.2. Preparation of EGFR Mutation-Specific Sea-Urchin-Like AuNCs. We improved the synthesis of sea-urchin-like AuNCs based on our previous method.[18] In a typical procedure, 10 mL of $HAuCl_4 \cdot 3H_2O$ aqueous solution (10 mM) was added to 10 mL of water in a 25-mL beaker with strong magnetic stirring. Then, 150 mg of AA powder was rapidly added to the water solution and allowed to react for 3 min. The as-prepared products were then centrifuged and washed with water and ethanol, respectively.

Functional molecules were conjugated with AuNC using our previous method.[17] A fresh prepared reporter solution (CV, 2×10^{-6} M) was added dropwise to a rapidly mixing AuNC colloid until the suspension achieving the highest SERS signal and minimal colloid aggregation. After 30 min, the HS-PEG-COOH was added dropwise to 2 mL AuNC−CV solution in an Eppendorf tube under rapid mixing. After 15 min of mixing, a large volume of mPEG-SH was added to the suspension to fill the areas not covered by HS-PEG-COOH. Afterward, the AuNC−CV-PEG-COOH was purified by three rounds of centrifugation (1000*g*) and resuspension in an ultrasonic PBS bath.

AuNC−CV-PEG-COOH was finally conjugated with EGFR E746_750 and L858R mutation-specific antibody. To active the COOH groups on the AuNC surface, freshly prepared ethyl dimethylaminopropyl carbodiimide (EDC) solution (50 mg/mL) and sulfo-NHS (50 mg/mL) were mixed vigorously for 20 min at room temperature. Excess EDC and NHS were separated from the suspension by three rounds of centrifugation (1000*g*) and resuspension in PBS. The AuNC with activated carboxyl groups were then reacted with EGFR mutation-specific antibodies at 25 °C for 2 h. The AuNC−EGFR (AuNC-E746_750 and AuNC-L858R) were purified by centrifugation and resuspension in PBS.

2.3. Physicochemical Characterization of AuNC. Transmission electron microscopy (TEM) micrographs were obtained, using a high-magnification electron microscope (Model H7650, Hitachi, Tokyo, Japan). Negative staining was used to observe the morphology characterization of the AuNCs. Ultraviolet−visible light (UV-vis) absorption spectra were recorded on a spectrometer (Model U-4100, Hitachi), using disposable polyacryl cuvettes. Nanoparticle size was analyzed by the dynamic light scattering (DLS) through a Malvern Zetasizer Nano ZS-90 at 25 °C, in water. Zeta potential was determined using a Malvern Zetasizer Nano ZS-90 at 25 °C in 0.1 M KCl solution. The Bradford assay, which is a colorimetric protein assay, was based on an absorbance shift of Coomassie Brilliant Blue dye where, under acidic conditions, the red form of the dye was converted to its bluer form to bind to the protein being assayed.[23] Standard addition calibration curve was used for the interpolation of the samples containing the excess peptide that was not bound to nanoparticles. Raman spectra data were recorded on a Labram HR 800 (Horiba Jobin-Yvon). The laser beam was set at 17 mW with 633-nm He−Ne laser radiation and accurately focused on a 1 μm^2 spot on the surface of the sample. The acquisition period was 20 s, with a spectral

DOI: 10.1021/am508122e
ACS Appl. Mater. Interfaces 2015, 7, 359−369

resolution of 1 cm^{-1} over a Raman shift range of 700−1800 cm^{-1}. Raman spectrum of liquid was taken in a cuvette. The H1650 cancer cells were fixed with 4% paraformaldehyde, then centered and photographed using 10× objective magnifications, and measured using 100× objectives.[24]

Sea-urchin-like AuNC (~600 nm) and spherical Au nanoparticles (~90 nm) were synthesized as described in previous research[18,25] (see details in S1.1 and S1.2 in the Supporting Information). The diluted sea-urchin-like AuNC (~90 nm and ~600 nm, respectively) and spherical Au nanoparticles (~90 nm) aqueous solution were deposited dropwise onto a silicon (Si) substrate and kept dry in air. For the measurements of individual nanoparticles, 100 μL of the 2×10^{-5}, 2×10^{-6}, and 2×10^{-7} M CV aqueous solution were deposited dropwise onto 1 cm × 1 cm Si substrate, which was kept in a petri dish covered with aluminum foil to allow it to dry in air. The SERS signals were randomly acquired from 25 spots of the substrate. The excitation laser spot size was 1.0 μm under a high-resolution 100× objective. The acquisition time of spectra and laser power for the characterization of single particle were 20 s and 0.047 mW, respectively, using a 1/100 filter.

2.4. Distribution and Characteristics of AuNC-EGFR in Living Cells. Human lung adenocarcinoma cell line A549, H1975, and H1650 were obtained from ATCC (Manassaa, VA, USA), and cultured in a RPMI-1640 medium (Gibco, USA) with 10% fetal bovine serum (Hyclone, USA) at 37 °C with 5% CO_2 in humidified incubators. Cells were seeded in a 10-cm-diameter petri dish at a density of 1×10^5 cells cm^{-2} and grown to 80% confluence in a growth medium. To minimize nonspecific binding or nanoparticle internalization and maximize the SERS signal, the cells were gently mixed and co-cultured with the AuNC-EGFR (2.35×10^9 counts) for 2 h. The growth medium was then aspirated and the remaining cells were washed with 4 °C PBS for three cycles. The cells was removed from the petri dish by gentle scraping, transferred to a 15-mL universal tube, and centrifuged at 92*g* (4 °C) for 5 min. The cells were resuspended in 2.0 mL of PBS before SERS measurement, TEM analysis, and inductively coupled plasma mass spectrometry (ICP-MS) detection.

The cancer cells were fixed in 3.0% glutaraldehyde solution at 4 °C for 2 h, then rinsed (for 30 min) in a PBS buffered solution (0.1 M, pH 7.4), and post-fixed in 1% osmic acid solution for 1 h. After dehydration in an ethanol gradient (70%, 95%, and 100% ethanol for 20 min, respectively), samples were embedded in epoxy resin and then were stained with uranylacetate and lead citrate. Sections were examined under TEM examination (Model H7650, Hitachi).

For immunofluorescence (IF) staining, the cells were first fixed in 4% paraformaldehyde for 30 min at room temperature. They were rinsed with PBS and blocked for 1 h in 3% bovine serum albumin at room temperature. The cells then were incubated with secondary antibody (antigoat-fluorescein isothiocyanate (FITC), 1:100) in darkness at 37 °C for 50 min. Finally, stained cells were visualized under a laser confocal microscope (Model TCS SP8, Leica Co., Germany).

The mass of gold in the cancer cells was analyzed by an Elan 9000 ICP-MS (Perkin−Elmer, Inc., Waltham, MA, USA). After centrifugation, dried pellets of AuNC-incubated H1650 cells were digested with aqua regia (450 μL of hydrochloric acid and 150 μL of nitric acid, purified by sub-boiling) for 2 h and sonicated at 80 °C for 2 h. The cell digests were diluted to 100 mL with ultrapure water for ICP-MS analysis. For calibration by standard addition, gold chloride was diluted with water to yield Au standards of 1, 5, 10, 50, 100, 500, 1000, 5000, 10000 ng/L. Blanks without and with cells (without AuNC) were prepared after the same procedure. ^{236}Bi (100 ng/L) was used as an internal standard.

2.5. Preparation of Clinical MPE Samples. From January 2012 to December 2013, 154 patients with lung adenocarcinoma were collected consecutively in this study. All patients were ethnic Chinese (Han). Of these, 35 patients were finally selected for this study, based on the following criteria: pathologic diagnosis of stage IV lung adenocarcinoma, depending both tissues and exfoliative cells of MPE; availability of a sufficient amount of MPE for IHC and SERS analysis; and presence of a sufficient amount of cancerous tissues (biopsied using a bronchoscope) that contained a minimum of 50% tumor cells for real-time PCR. The study protocol has been approved by the Institutional Review Board and Research Ethical Board, Fourth Military Medical University, and a written informed consent was obtained from each participant before the initiation of any study-related procedure. All cases were reviewed by pathologists for confirmation of adenocarcinoma. The histology was based on the criteria of the World Health Organisation, and the TNM (Tumor, Node, and Metastasis) stage was determined according to version 7 of International Association for the Study of Lung Cancer (IASLC) staging system.

A quantity of 400 mL of MPE was collected through needle thoracentesis in each patient. MPE samples were collected using an evacuated sterile vial containing sodium heparin and polyester gel. After removing the red blood cells through the use of a red blood cell lysis buffer and inhabiting coagulation, the fresh MPE was centrifuged at room temperature for 5 min at 92*g*. After centrifugation, the low density cell layer containing lymphocytes, monocytes, and exfoliative cells was transferred into a new tube and washed with PBS. The cells were counted and split into two samples. One sample was incubated with AuNC-EGFR (2.35×10^9 counts), with constant mixing for 2 h at 37 °C. Then, the cells were washed with ice-cold PBS three times and resuspended in 2 mL PBS for SERS measurement. The other sample was prepared for H&E and IHC analyses.

2.6. EGFR Mutation Analysis. Genomic DNA was extracted from lung cancer cells and tissues as per standard protocols (E.Z.N.A Tissue DNA Kit, Omega, USA). The genomic DNA was tested by using an ADx EGFR Mutations Detection Kit (Amoy Diagnostics, Xiamen, China), which has received approval from the State Food and Drug Administration (SFDA) for clinical usage in mainland China. The kit used the principle of amplified refractory mutation system (ARMS) and detected 29 mutations in exon 18 (G719A, G719S, G719C), exon 20 (T790M, S768I), and exon 21 (L858R, L861Q), and 19 deletions in exon 19. The assay was carried out according to the manufacturer's protocol with the MX3000P (Stratagene, La Jolla, USA) real-time PCR system. A positive or negative result could be reached if it met the criterion that was defined by the manufacturer's instructions. The Ct values used to determine if a sample was positive or negative were based on extensive validation. The Ct values that we used to determine whether a sample was positive or negative were based on the following extensive validation: strong positive, if $Ct < 26$; weak positive, if $26 < Ct < 29$; negative, if $Ct > 29$.

2.7. Data Preprocessing and Statistical Analysis. The raw spectrum was preprocessed by a first-order Savitsky-Golay filter (7 points) for noise smoothing, and then a fifth-order polynomial was found to be optimal for fitting the autofluorescence background in the noise-smoothed spectrum. This polynomial was then subtracted from the noise-smoothed spectrum to yield only the tissue Raman spectrum. The processed data was used in the following steps. Principal component analysis (PCA) and the support vector machine (SVM) algorithm were developed as a diagnostic algorithm for prediction in Matlab7.1 (The Mathworks, Inc., Natick, MA). PCA is a data compression procedure that found major trends within the spectral dataset and redefined the dataset using a small set of component spectra or principal components (PCs) and scores.[24] The first three PCs represented the importance and highest variance of the dataset. In this study, PCA was employed to highlight the major variability existing in the spectral dataset, especially recording on the edge of the detection threshold. SVM with a radial basis function kernel and a particle swarm optimization solver were utilized to identify different groups in the form of their PC scores.[26] PCA/SVM algorithm was trained and tested by using leave-one-spectrum-out cross-validation. In this procedure, a SVM model was originally built from all but one spectrum. The model then predicted the category of the omitted spectrum and stored the result. This procedure was repeated with each omitted spectrum, discriminating each spectrum in turn. Finally, a probability of prediction was calculated and expressed as a sensitivity and specificity for each group. The coefficient of variation (COV) was defined as the ratio of the standard deviation to the mean. Linear correlation and regression analysis were performed to test the

DOI: 10.1021/am508122e
ACS Appl. Mater. Interfaces 2015, 7, 359−369

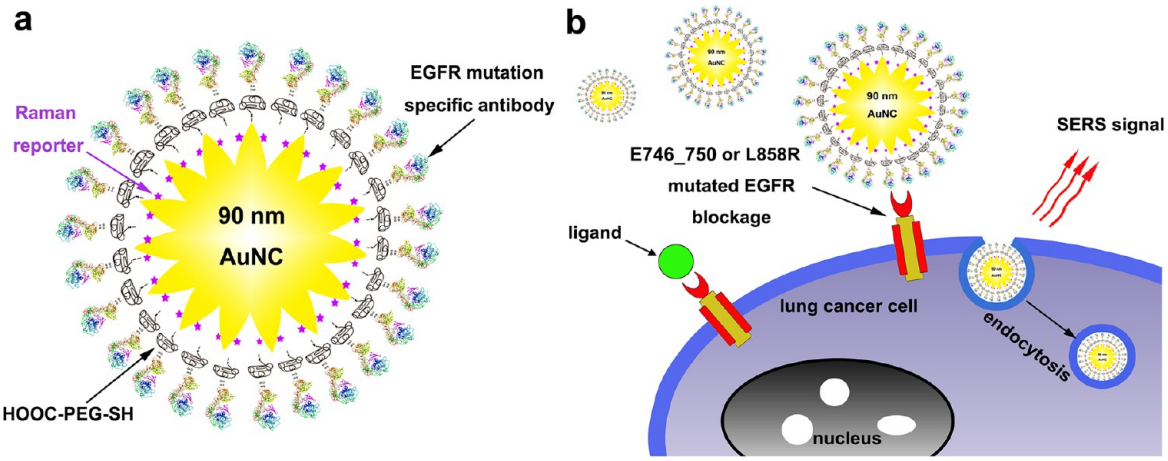

Figure 1. (a) Schematic illustration of the procedure employed for the fabrication of SERS-active AuNC-EGFR. (b) The AuNC-EGFR could easily bind to mutated EGF receptors, entering into the cancer cells by endocytosis.

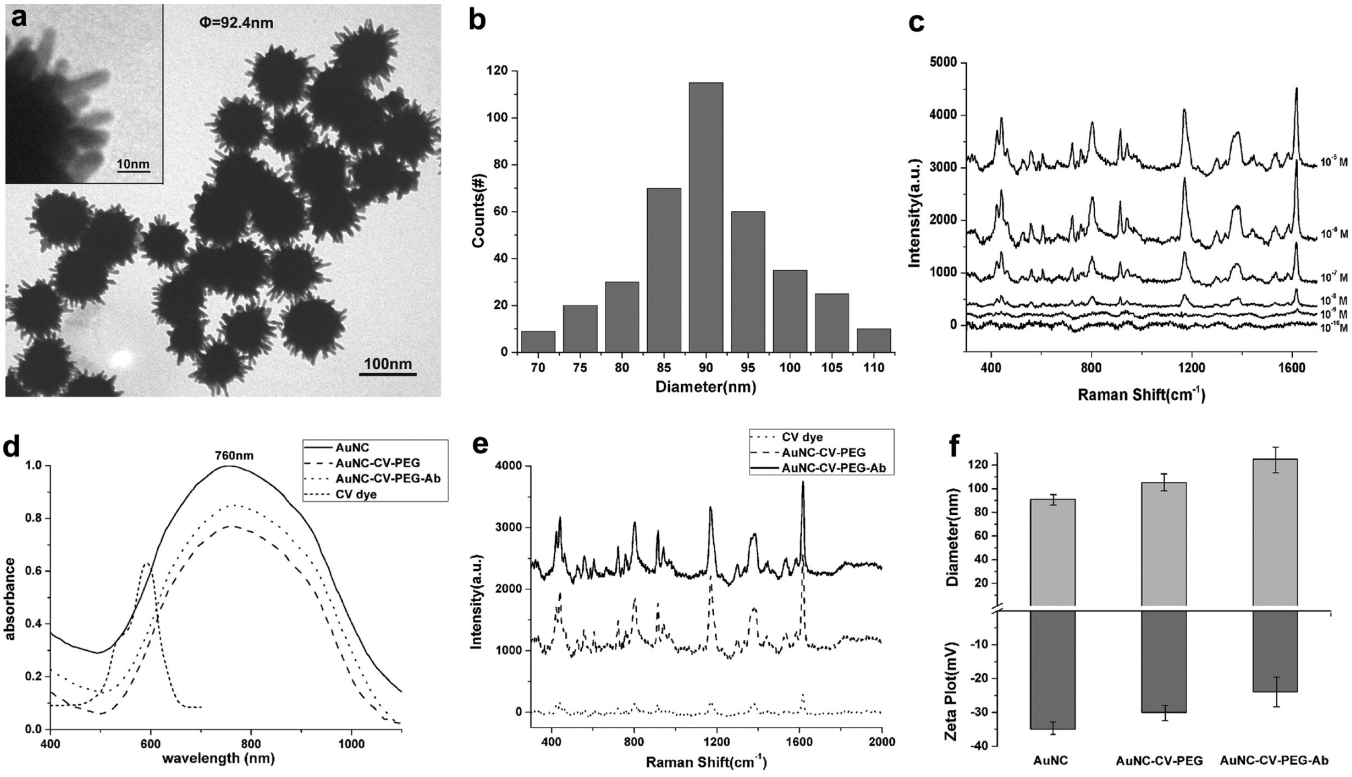

Figure 2. Physicochemical characterization of tested AuNCs: (a) TEM image of sea-urchin-like AuNCs, with an average diameter of 92.4 ± 11.2 nm; (b) particle size distribution of superficial nanopricks with an average length of 15 nm (scale bar, 10 nm); (c) SERS spectra of individual AuNC performed with a 633-nm excitation laser, and CV molecule concentrations from 2×10^{-5} M to 2×10^{-10} M (from top to bottom); (d) optical extinction spectra with an SPR band centered at 760 nm (also shown was a CV absorbance spectrum with characteristic peaks at 602 nm); (e) Raman spectra of AuNC-EGFR with a characteristic SERS peak at 1617 cm^{-1}; and (f) hydrodynamic light scattering in water and zeta-potential data of all AuNC-EGFR.

relationship of two independent variables. A Student's *t*-test was performed to compare the SERS intensities at 1617 cm^{-1} between different numbers of cells. *P* values of <0.01 were considered significant.

3. RESULTS AND DISCUSSION

3.1. Synthesis and Characterization of SERS-Active Sea-Urchin-Like AuNC-EGFR. As shown in Figure 1a, the biocompatible SERS-active sea-urchin-like AuNC-EGFR was synthesized in this study. Highest SERS signals and minimal colloid aggregation determined the usage of CV during the coating process, resulting in the favorable SERS detection property. The CV molecules were adsorbed to the negatively charged AuNC through electrostatic interaction, a weak intermolecular force. The thiol-PEG can prevent desorption or enzymatic degradation of CV from nanoparticles under very harsh conditions, including strong acids (0.1 M HCl), strong bases (0.1−1 M NaOH), concentrated salts (1−2 M NaCl) and organic solvents (methanol, ethanol, and dimethyl sulfoxide).[15,16] Hence, α-mercapto-ω-carboxy PEG solution (HS-PEG-COOH) was added in 10-fold excess to the AuNC−CV,

DOI: 10.1021/am508122e
ACS Appl. Mater. Interfaces 2015, 7, 359−369

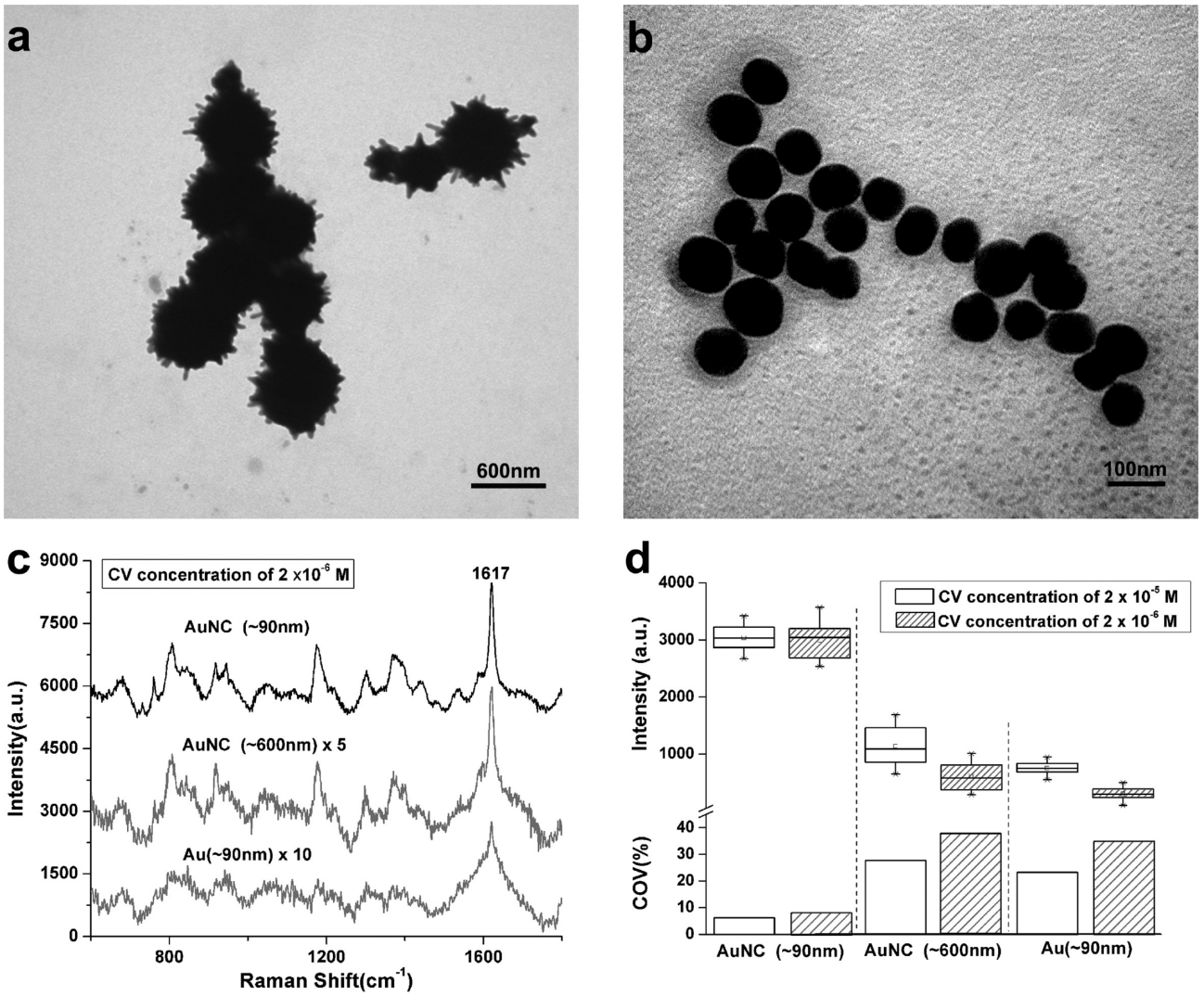

Figure 3. TEM images of (a) AuNC with a diameter of ~600 nm and (b) spherical Au nanoparticles with a diameter of ~90 nm. (c) SERS spectra of CV molecules emitted from AuNC (~90 nm), AuNC (~600 nm), and spherical Au nanoparticle (~90 nm), respectively. (d) Box plots and coefficient of variation (COV) values of the SERS signal at 1617 cm^{-1} emitted from AuNC (~90 nm, ~600 nm) and spherical Au nanoparticles (90 nm), respectively.

in order to fully cover the AuNC−CV and to stabilize the gold conjugates against aggregation and desorption, while increasing biocompatibility, grant chemical functionality and avoiding opsonization. After PEG functionalization, EGFR mutation specific antibody was conjugated to the AuNC−CV-PEG-COOH by coupling reaction between the carboxylated PEG spacer and the amine terminal group of the antibody using an EDC/NHS as dehydration agents. This biocompatible AuNC-EGFR could easily bind the mutated EGFR blockage and enter into the cancer cells by endocytosis (Figure 1b).

TEM and dynamic light scattering (DLS) analysis showed the AuNC with an average diameter of 92.4 ± 11.2 nm, which was composed of some nanopricks with an average length of 15 nm (see Figures 2a and 2b). Similar to our previous experiment,[18] the AA content and reaction time had important influence on the resulting products. After increasing the content of AA, more and longer nanopricks formed, which might dramatically increase the excitation cross-section and the electromagnetic field enhancement. Meanwhile, shortening the reaction time resulted in smaller size AuNC. The SERS signals were measured using a 633-nm He/Ne laser with CV molecule concentrations ranging from 2×10^{-5} to 10^{-10} M (Figure 2c). Actually, the maximum and minimum SERS signals were obtained at concentrations of 2×10^{-6} M and 2×10^{-9} M, respectively. Thus, final CV concentration for coating process on the AuNC was confirmed at 2×10^{-6} M. According to the algorithm of EF in previous experiments[27] for the CV molecules, the average EF for the individual AuNC was estimated to be ~1.97×10^7 under the 633-nm excitation wavelength (see details in Section S2.1 in the Supporting Information). The improved nanoclusters showed several remarkable advantages. First, the AuNC presented a higher density of nanopricks, which might dramatically increase the excitation cross-section and the electromagnetic field enhancement.[27] Second, the smaller particle size made it easy to obtain the overall SERS signal from the entire AuNC irradiation using a He−Ne laser 1 μm in diameter, resulting in high uniformity and reproducibility.

Figure 2d presented the UV-vis spectra of the AuNC in ultrapure water. The absorption peak of the original AuNC colloids reached at 760 nm. The absorption peak remained almost unchanged during the entire coating process (with a

DOI: 10.1021/am508122e
ACS Appl. Mater. Interfaces 2015, 7, 359−369

shift in 2−3 nm, partially due to the slight aggregation and characteristic extinction spectra of Raman reporter). The typical Raman spectrum acquired from the Raman reporter (CV dye) only, AuNC−CV, and AuNC−CV-Ab-PEG are depicted in Figure 2e, which showed a characteristic SERS peak at 1617 cm^{-1}. The thiol-PEG-coated AuNC became so stable that their SERS signals do not change under the coating process. The hydrodynamic diameter of particles increased by ∼15 nm after PEGylation. A considerable increase in diameter was observed upon EGFR mutation-specific antibody binding (increased ∼21 nm) as measured by DLS in water. The size distribution determined by DLS was based on intensity distributions (Figure 2f). Zeta-potential data showed that all nanoparticles conjugates were considered anionic, with zeta potentials between −25 mV and −35 mV. The standard addition calibration curve of antibody was depicted by using the Bradford assay (see Figure S1 in the Supporting Information). The amount of excess antibody in supernatants that was not bound to AuNCs was achieved using this calibration curve. Thus, 312.4 ± 12.2 antibodies per nanoparticle were calculated as previously described.[17,23]

To assess the improved SERS activity of this nanocluster, we developed previous sea-urchin-like AuNC (∼600 nm, Figure 3a) and spherical Au nanoparticles (∼90 nm, Figure 3b) and compared the uniformity and reproducibility between three types of nanoparticles. Approximate 15−19 AuNCs on the Si substrate can be covered under a laser spot size of 1.0 μm, which was also beneficial to achieve uniform SERS signals. As shown in Figure 3c, the SERS signals on the Si substrate can be identified at the CV concentration of 2×10^{-6} M for individual AuNC (∼90 nm), which, in contrast, were ∼5-fold and ∼10-fold larger, with regard to intensity of AuNC (∼600 nm) and Au nanoparticle (∼90 nm), respectively. The COV value of SERS intensity at 1617 cm^{-1} from 25 random spots on the Si substrate was calculated to evaluate the uniformity and reproducibility of SERS signals (Figure 3d). The particle size and SERS activity of the AuNC (∼90 nm) can contribute to the remarkable uniformity and reproducibility, with COV values of 7.0% and 9.7% at CV concentrations of 2×10^{-5} M and 2×10^{-6} M, respectively. For AuNC (∼600 nm), the COV values can increase to 30.4% and 38.2% for 2×10^{-5} M and 2×10^{-6} M, respectively. Also, the COV values of Au nanoparticles (∼90 nm) were 24.6% and 36.4% for 2×10^{-5} M and 2×10^{-6} M, respectively. It was worth noting that super signal amplification and small particle size might be a key factor of uniformity and reproducibility.

3.2. Lung Cancer Cell Targeting and the Intracellular Disassembly of the AuNC-EGFR. Human lung cancer cell line A549, H1975, and H1650 were selected as the cell model. EGFR mutation analysis showed that H1975 carried the L858R mutation gene, H1650 carried the E746_750 mutation gene, and A549 carried wild-type (wt) EGFR gene (see details in Section S1.3 and Figure S2 in the Supporting Information). The bioconjugated AuNC-EGFR quickly bonded to the surface of H1975 or H1650 cells after incubating for 30 min, then gradually entered into cancer cells after 2, 6, and 12 h (see Figures 4a−d), as compared with control cells (A549) exhibiting few nanoparticles in the first 2 h. It was clearly seen that the AuNC-EGFR entered into the cells by endocytosis (see the black arrow in Figures 4b and 4c). Some co-localization was detected as AuNC-EGFR selectively accumulated in lysosomes of lung cancer cells. Also control cells incubated with the control AuNCs (coating with only mPEG-SH) were observed only in rare nanoparticles. To confirm the specificity of AuNC-EGFR, excess EGFR mutation-specific antibodies were preincubated with these cancer cells for binding the E746_750 or L858R receptor, and then these cells were co-cultured with AuNC-EGFR for 2 h. After three rounds of washing, the cells were bound with only a few AuNCs. These results demonstrated the specificity of AuNC-EGFR for entering into EGFR mutated cancer cells through endocytosis. Immunofluorescence staining was further performed to assess the activity of antibodies conjuncted on the nanoclusters. After being co-cultured with AuNC-E746_750 for 12 h, H1650 cells were incubated with secondary antibodies labeled with-FITC. Confocal microscopy images showed the bright fluorescence signals located mainly in cell membrane and cytoplasm (see Figure 4e). Although the strong acidic and enzymatic environment might result in the breakage of chemical bonds and stimulate the dissociation of the multifunctional nanoclusters inside the endocytic organelles,[28,29] the fluorescence signal was still detectable and high, at least after 24 h of cell

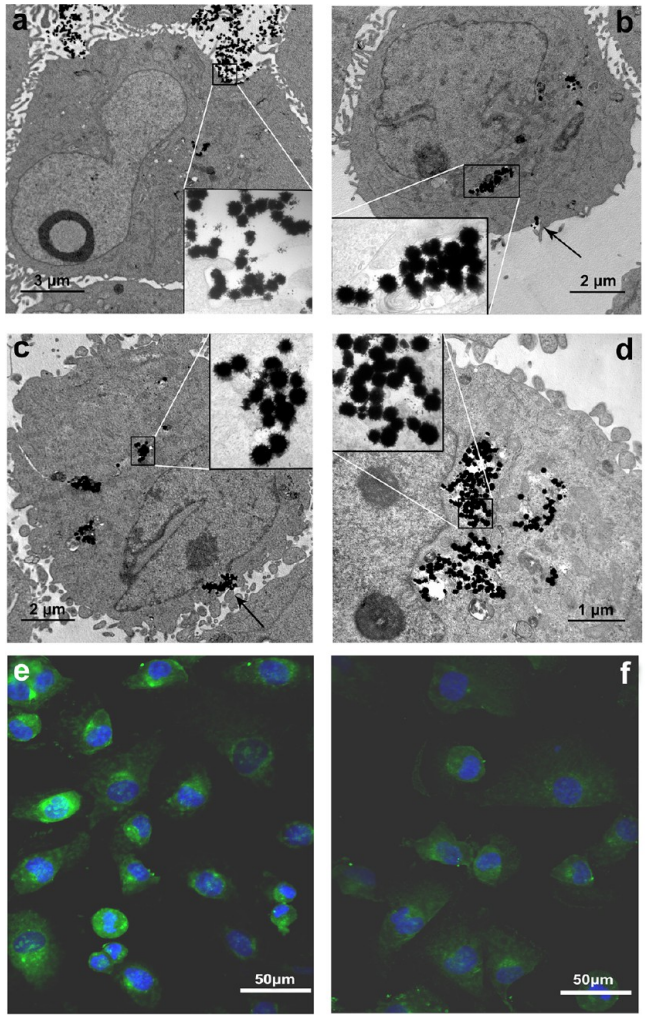

Figure 4. TEM images showed that the bioconjugated AuNC-E746_750 (a) was quickly bound to the surface of the H1650 cell after incubating for 30 min and then (b−d) entered into the cancer cells for 2 h (panel (b)), 6 h (panel (c)), and 12 h (panel (d)). Black arrows shown in panels (b) and (c) indicate where the process of endocytosis is occurring. The laser confocal microscopy image showed the fluorescein isothiocyanate fluorescence of the H1650 cells after being incubated with the AuNC-E746_750 for (e) 12 h and (f) 24 h.

DOI: 10.1021/am508122e
ACS Appl. Mater. Interfaces 2015, 7, 359−369

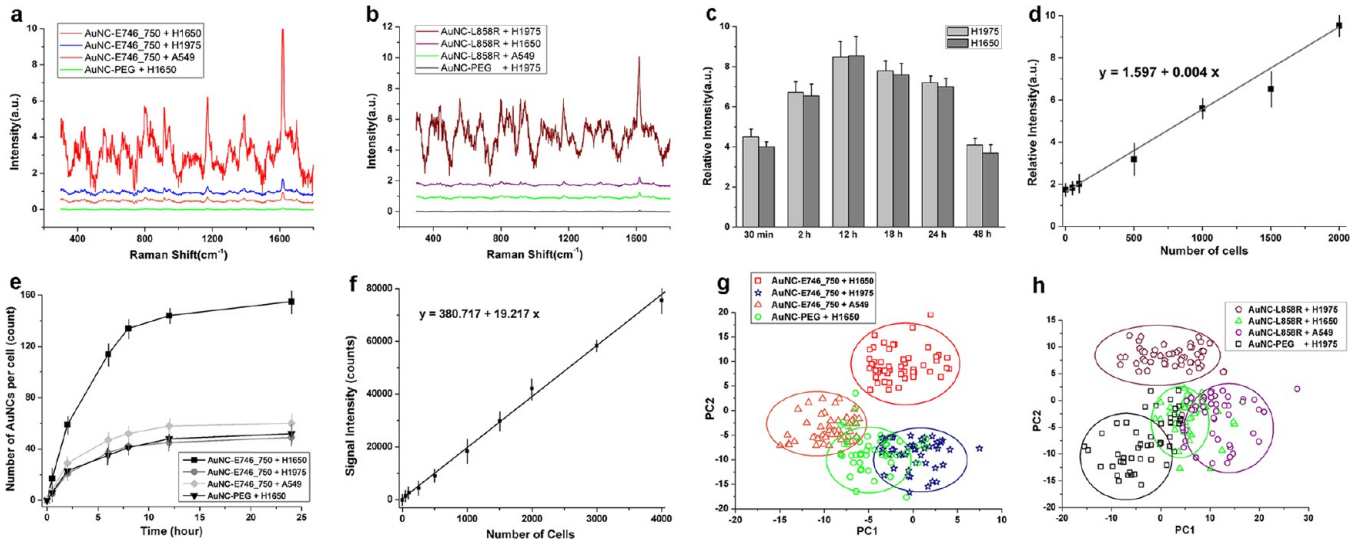

Figure 5. (a) SERS spectra of AuNC-E746_750-labeled H1650 (red), H1975 (blue), and A549 (red-brown) cells, and AuNC-PEG-labeled H1650 cells (green); (b) SERS spectra of AuNC-L858R-labeled H1975 (brown), H1650 (purple), and A549 (green) cells, and AuNC-PEG-labeled H1975 cells (black); and (c) SERS signal at 1617 cm^{-1} of the AuNC-EGFR labeled cancer cells for 30 min, 2 h, 12 h, 18 h, 24 h, and 48 h. (d) The linear regression curve between SERS signals at 1617 cm^{-1} and the number of AuNC-E746_750-labeled H1650 cells (0, 50, 100, 500, 1000, 1500, and 2000). (e) Cellular uptake of AuNC-E746_750, as a function of incubation time. (f) The linear regression curve between ICP-MS signals and the number of AuNC-E746_750-labeled H1650 cells (0, 50, 100, 250, 500, 1000, 1500, 2000, 3000 and 4000). (g) Scatter plot of the spectra from AuNC-E746_750-labeled H1650 cells (open red squares, □), H1975 (open blue stars, ☆), A549 (open red-brown triangles, △) cells, and AuNC-PEG-labeled H1650 cells (open green circles, ○); the similarly colored ovals indicate the outline of scatter distribution between the four subtypes. (h) Scatter plot of the spectra from AuNC-L858R-labeled H1975 (open brown pentagons, ⬠), H1650 (open green triangles, △) and A549 (open purple circles, ○) cells, and AuNC-PEG-labeled H1975 cells (open black square, □); the similarly colored ovals indicate the outline of the scatter distribution between the four subtypes. PC = principal component.

incubation (see Figure 4f). It can be observed that the activity of the EGFR mutation-specific antibody was retained after conjugation to the nanoclusters.

3.3. Detection Sensitivity and Specificity of AuNC-EGFR. To exclude subjectively selective location of cancer cells, all spectra were detected in solution (see Figure S3a in the Supporting Information). However, this resulted in a loss of detection sensitivity due to a decrease in the enhancement capability of AuNC in water.[27] In our previous study,[24] Raman spectra were compared in cancer cells and tissues between wt-EGFR and E746_750, L858R mutation. The signal peaks at 675, 1107, 1127, and 1582 cm^{-1} assigned to specific amino acids and DNA were significantly increased in wt-EGFR cells. While the peaks at 1085, 1175, and 1632 cm^{-1} assigned to arginine were slightly increased in L858R cells. The signal of E746_750 cells was weaker than others due to exon 19 deletion that removes residues 746−750 of the expressed protein. However, the signals directly from cells were very weak, resulting in being overlapped by the strong SERS signals of AuNCs. The characteristic spectra of CV remained unchanged after incubating with cancer cells for 2 h (see Figure S3b in the Supporting Information). The AuNC-EGFR-labeled H1975 or H1650 cells exhibited the strong fingerprint SERS signals of the Raman reporter, while significantly weak SERS signals were detected from the H1975 or H1650 cells that were exposed to nontargeted AuNC and A549 cells incubated with targeted AuNC (see Figures 5a and 5b). These weak SERS signals from control cells (A549) and control nanoparticles (nontargeted AuNC) were probably caused by residual nanoparticles in the cell suspension, nonspecific binding, or nanoparticle internalization.

The AuNC-EGFR-labeled H1975 or H1650 cells showed a characteristic and strong Raman peak at 1617 cm^{-1}, which gradually increased to the highest level until being co-cultured for 12 h (Figure 5c). The AuNC-EGFR-labeled A549 cells exhibited very weak signal in the first 2 h, but the SERS signal significantly increased until 12 h, because of nonspecific binding or nanoparticle internalization, which could be explained by different SERS enhancement factors, depending on the aggregate morphology and the interparticle distance.[30] To minimize the nonspecific binding and maximize the SERS signal, all AuNC-EGFR were incubated with cancer cells for 2 h. Since the dissociation of the multifunctional nanoparticles inside the strong and enzymatic environment, the Raman reporter was detached from the nanoparticles, resulting in gradually reduced SERS signal. To determine assay sensitivity, 0, 50, 100, 500, 1000, 1500, and 2000 H1650 cells mixed with A549 cells were co-cultured with AuNC-E746_750 for 2 h. A linear correlation between the number of cells and the SERS signal at 1617 cm^{-1} was found, and the linear regression equation is indicated in Figure 5d. Except for a subgroup of 50 cells, significant differences ($P < 0.01$) in the SERS signal were found between a subgroup of 100−2000 cells and the control group (cell 0). Thus, the limit of detection was 50 cells in a 2-mL suspension (25 counts/mL).

The gold nanoparticles entered into the cells via the receptor-mediated endocytosis pathway, and the unbound or available receptors determined whether and how much a molecule or nanoparticle entered a cell via this mechanism.[31] ICP-MS showed that the uptake of the AuNCs significantly increased for the first 2 h in Figure 5e, but the uptake rate gradually reached a plateau at 8−12 h, when ranging the maximum receptors on the cell surface. It was worth noting that the AuNC-E746_750-labeled H1650 cells contained much more AuNCs than other control cells, which could be attributed to the EGFR mutation targeting of these nano-

DOI: 10.1021/am508122e
ACS Appl. Mater. Interfaces 2015, 7, 359−369

clusters.[32,33] The mass of gold in single H1650 cells exposed to AuNCs-E746_750 for 2 h was 220.0 ± 11.4 pg, which was calculated as ~59 ± 3 AuNCs per cell (see details in Section 2.2 in the Supporting Information), and the COV values for five replicate detection measurements of gold mass per cell were 4.2%. The number of nanoclusters in the AuNC-E746_750-labeled H1975 and A549 cells and the AuNC-PEG-labeled H1650 cells was in the range of 21−28 per cell, resulting from residual nanoparticles and nonspecific binding (Figure 5e). The relationship between the Au signal intensity and number of the AuNC-E746_750 labeled H1650 cells is shown in Figure 5f, and a good linear relationship was obtained in the range of 50−4000 cells, which was in accordance with the relationship between SERS signals and cell number. However, SERS signals began to decline, although the gold mass in cells still ascended after 12 h. This behavior can be interpreted by detachment of CV and PEG molecules from the nanoclusters under the strong acidic and enzymatic environment in the lysosomes of cells.

It can be observed that SERS measurement is a signal-dependent identification for EGFR mutation status. It was difficult to identify an exact mutation status subjectively when the signals on the edge of the threshold were obtained. PCA and SVM were usually used for multidimensional data analysis and discrimination, and they methodologies were deemed to be efficient methods in the microdiagnosis of clinical samples.[24,26] Approximately 50 spectra were acquired for each subgroup. Figures 5g and 5h showed scatter plots of the first PC versus second PC of Raman spectra to demonstrate distinctive spectral clustering, in which each of the spectra has been represented by a different color and a different shape. The PCA/SVM diagnostic algorithm yielded an overall accuracy of 85.5% for differentiating AuNC-E746_750-labeled H1650 from other cells [i.e., sensitivity of 98.0% (49/50) and specificity of 78.0% (AuNC-PEG, 39/50), 84.0% (A549, 42/50), and 82.0% (H1975, 41/50)]. Similarly, the algorithm obtained an overall accuracy of 85.0% for differentiating H1975 from other cells after incubation with AuNC-L858R [i.e., sensitivity of 100.0% (50/50) and specificity of 74.0% (AuNC-PEG, 37/50), 80.0% (A549, 40/50), 86.0% (H1975, 43/50)].

3.4. Detection of EGFR Mutation Status of Exfoliative Cells in MPE. Table 1 shows the clinical characteristics of the 35 patients. EGFR mutations of cancer tissues were detected usign the ARMS method in 21 patients, including 12 of deletion in exon 19 and 9 of L858R mutations. The remaining 14 patients carried the wt-EGFR gene. After MPE was washed with PBS, the cell suspension, involving exfoliative cancer cells, white blood cells, etc., was analyzed by IHC and SERS. The ARMS method is a more sensitive detection procedure for EGFR mutation, while IHC can suggest a mutation status with a relatively high specificity.[5,34,35] To confirm the mutation status of exfoliative cells in the MPE samples, the EGFR mutation status of cancer tissues was detected by ARMS first, and the following IHC was further used to observe the morphology and mutation status of exfoliative cells. Although DNA sequencing was not further performed after EGFR mutation status was obtained using the ARMS method, IHC (using EGFR mutation-specific antibodies) can identify the E746_750 against other deletions in exon 19 in MPE samples. AuNC-EGFR was incubated with these cells suspension for 2 h, and then SERS signals were obtained in a 2-mL cell suspension washed by PBS for three cycles. Figure 6a showed that the SERS signal of mutated exfoliative cells was at least 10-fold stronger than that of the wt-EGFR cells. E746_750 and L858R mutation were expressed on the cytomembrane and cytoplasm (see Figure 6b, as well as Section 1.4 and Figure S4 in the Supporting Information). An average of 20 spectra was detected from each MPE sample. Figure 6c shows a scatter plot of the Raman spectra to demonstrate distinctively spectral clustering. It showed a significant classification between three mutation types of lung adenocarcinoma in a two-dimensional coordinate system. PCA/SVM algorithm predicted the mutation cells with an overall accuracy of 90.7% [i.e., sensitivities of 88.3% (E746_750, 212/240) and 87.8% (L858R, 158/180), and a specificity of 94.6% (wt-EGFR, 265/280)].

Table 1. Clinical Characteristics of 35 Patients with Stage IV Lung Adenocarcinoma

characteristic	non-mutation	L858R	E746_750
number of patients	14	9	12
age (mean, years)	67.7	59.3	60.5
sex (no, male/female)	9/5	4/5	6/6
differentiation			
poor	3	3	5
good	6	3	3
moderate	5	3	4

To date, several methods are available for EGFR mutation detection on cytologic samples. Nonsequencing-based procedures—for example, high-resolution melting and restriction fragment length polymorphism analysis—can be used for mutation screening and can give indirect evidence of the mutation status.[7] Other sequencing-based methods, such as peptide nucleic acid-locked PCR clamping, allele-specific quantitative real-time PCR, and scorpion ARMS, can provide accurate identification of the type and sites of mutation. The main limitation of these methods is that they need multiple PCRs, and an adequate amount of genomic DNA, which is not always available while working with cytologic samples.[7,8] To overcome this deficiency, SERS was first used for EGFR mutation detection in this research. The AuNC-EGFR could bind actively to EGFR-mutated exfoliative cancer cells in MPE, and then emit a strong SERS signal. As compared with other test methods,[36] SERS detection presented a significant higher sensitivity and specificity. This might be attributed to

(1) SERS was an enhanced signal, depending on the sea-urchin-like AuNC, having the advantage for the detection of trace cells.
(2) Preparation of the MPE specimen for SERS was much simpler than for PCR, resulting in a minimal loss of cancer cells in the preparation process.
(3) The SERS signal was obtained in solution objectively, thereby reducing the number of subjective errors as much as possible.

There are several limits of the SERS measurement for EGFR mutation. Similar to the restriction of IHC, IF, Western blot, coimmunoprecipitation, and other test methods that rely on antibodies, SERS measurement is also dependent on the antibodies or ligands conjugated on the nanoparticles. The EGFR mutation-specific antibodies (Catalog Nos. 2085 and 3197, Cell Signaling Technologies, USA) were widely used to predict the E746_750 and L858R mutation status elsewhere.[5,34,35] Antibodies that are directed toward other rare mutation subtypes, such as L861Q, T790M, and S768I, have

DOI: 10.1021/am508122e
ACS Appl. Mater. Interfaces 2015, 7, 359−369

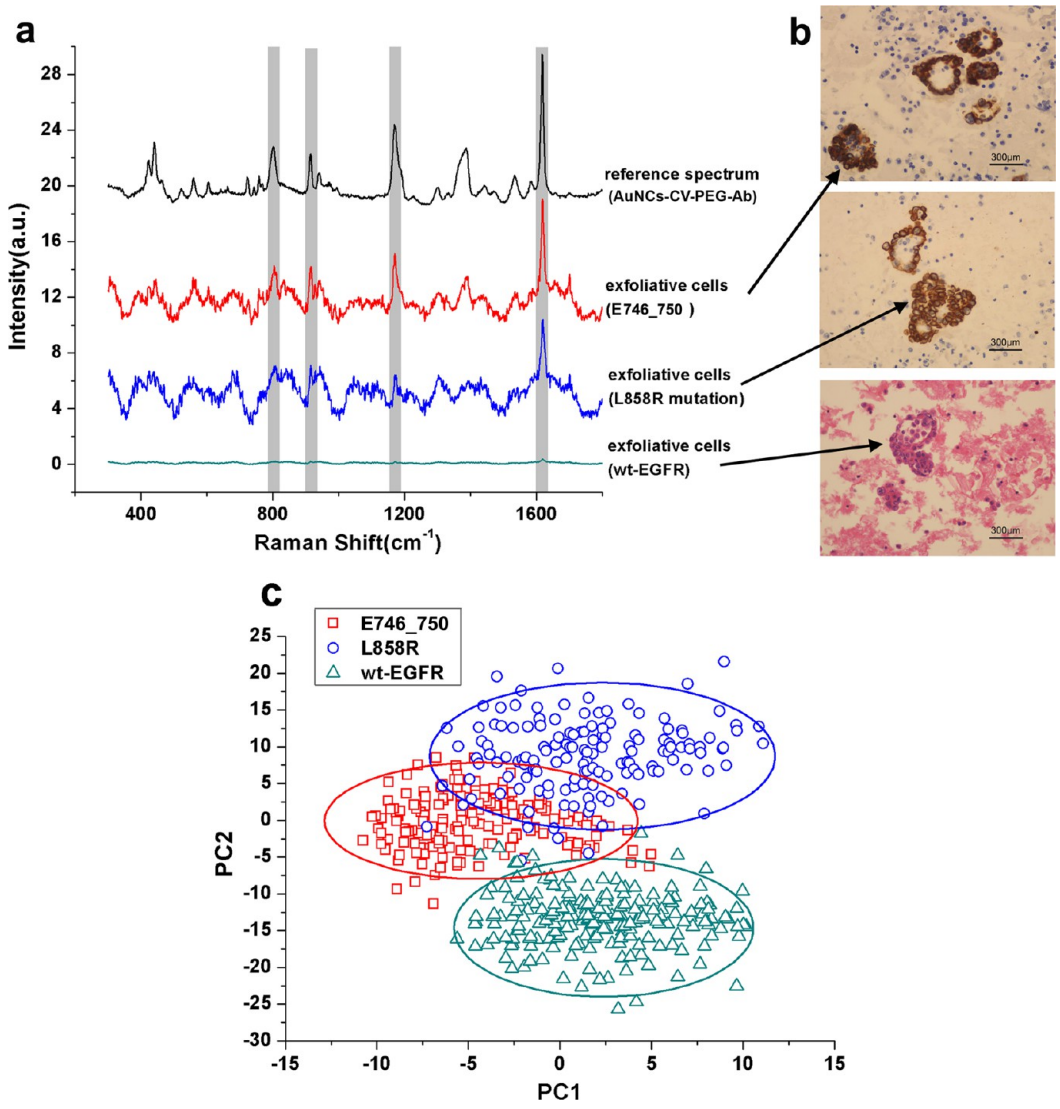

Figure 6. (a) SERS spectra of the AuNC-EGFR (black, reference spectrum), AuNC-E746_750- or L858R-labeled exfoliative cells (red line, E746_750; blue line, L858R; and green line, wt-EGFR). (b) IHC staining of exfoliative cell samples with E746_750 mutation (score 3+), L858R mutation (score 3+), and wt-EGFR. (c) Scatter plot of the spectra from wt-EGFR (open green triangle, △), L858R (open blue circle, ○), and E746_750 (open red square, □) exfoliative cells used to develop the model projected onto a plane in PC. The colorful elliptic shadow gave the outline of scatter distribution between three mutation types. PC = principal component.

not been developed yet. In addition, the ADx EGFR Mutations Detection Kit being used in the research can test 19 deletions in exon 19, but the EGFR mutation-specific antibodies (Catalog No. 2085) can only detect the most-frequent deletion of E746_750. Thus, the SERS method can only detect E746_750 and L858R mutation. However, as shown in previous reports,[12,13,15,16] it can be assumed that SERS is also able to detect the other EGFR mutation if the specific antibodies are coated on the nanoparticles. Second, the threshold of SERS was confined as 25 cells per mL because of nonspecific binding or nanoparticle internalization. A reduction in nonspecific binding by using some inhibitor of independent endocytosis, or an increase in specific binding through cell-penetrating peptides, may be the efficient improvement of the detection threshold. Because of the rigorous inclusion criteria, involving stage IV adenocarcinoma, which are abundant in MPE samples (the existence of mutated cancer cells in MPE has been established), only 35 clinical samples were finally selected in this research. The low detection rate of exfoliocytology examination in MPE and invasive needle thoracocetesis prevent more samples from being used.

4. CONCLUSION

In summary, we synthesized the sea-urchin-like AuNC with more and longer nanopricks, which exhibited an improved enhancement factor (EF) of 1.97×10^7. After being capped with CV, EGFR mutation-specific antibodies, and PEG, the AuNC-EGFR had excellent biocompatibility and EGFR mutation-targeted recognition in lung cancer cell suspension. The SERS signal at 1617 cm^{-1} was linear correlated with the number of cancer cells, demonstrating the minimum detection limit as 25 cells in a 1-mL cell suspension. The mass of gold in single H1650 cells exposed to AuNC-E746_750 ranged from 208.6 pg to 231.4pg, which approximately corresponded to 56–62 AuNC per cell. Furthermore, this AuNC-EGFR was preclinically utilized for EGFR mutation detection in MPE, yielding a superior accuracy of 90.7%. SERS detection based on sea-urchin-like AuNC is an efficient method for EGFR

DOI: 10.1021/am508122e
ACS Appl. Mater. Interfaces 2015, 7, 359–369

mutation detection in MPE, and may show great potential in applications such as predicting gene typing of clinical lung cancer in the near future.

■ ASSOCIATED CONTENT

Supporting Information

This material is available free of charge via the Internet at http://pubs.acs.org.

■ AUTHOR INFORMATION

Corresponding Authors

*E-mail: hljyxq@fmmu.edu.cn (L. Huang).
*E-mail: lxfchest@fmmu.edu.cn (X. Li).
*E-mail: dxcui@sjtu.edu.cn (D. Cui).

Author Contributions

[∇]These authors contributed equally to this paper.

Funding

The National Natural Science Foundation of China (through Nos. 81370115 and 81000938) and the Science and Technology Innovation Development Fund of Tangdu Hospital of The Fourth Military Medical University are acknowleged for providing financial support of this work.

Notes

The authors declare no competing financial interest.

■ ACKNOWLEDGMENTS

The authors thank Professor You Liu and Liqing Huang (School of Science, Xi'an Jiao Tong University, China), for the help with SERS Theory; Shanghai Fenglin Clinical Laboratory Co., Ltd., for the help with ICP-MS detection; Jiayan Liu (Department of Pathology, Xijing Hospital, the Fourth Military Medical University), for her good job of pathologic experiment; and Miaomiao Wen (Department of Thoracic Surgery, Tangdu Hospital, the Fourth Military Medical University), for her help with culturing cells.

■ REFERENCES

(1) Siegel, R.; Ma, J.; Zou, Z.; Jemal, A. Cancer Statistics, 2014. *Ca—Cancer J. Clin.* **2014**, *64*, 9−29.

(2) Beadsmoore, C. J.; Screaton, N. J. Classification, Staging and Prognosis of Lung Cancer. *Eur. J. Radiol.* **2003**, *45*, 8−17.

(3) Hirsch, F. R.; Bunn, P. A., Jr. EGFR Testing in Lung Cancer Is Ready for Prime Time. *Lancet. Oncol.* **2009**, *10*, 432−433.

(4) Mok, T. S.; Wu, Y. L.; Thongprasert, S.; Yang, C. H.; Chu, D. T.; Saijo, N.; Sunpaweravong, P.; Han, B.; Margono, B.; Ichinose, Y.; Nishiwaki, Y.; Ohe, Y.; Yang, J. J.; Chewaskulyong, B.; Jiang, H.; Duffield, E. L.; Watkins, C. L.; Armour, A. A.; Fukuoka, M. Gefitinib or Carboplatin−Paclitaxel in Pulmonary Adenocarcinoma. *N. Engl. J. Med.* **2009**, *361*, 947−957.

(5) Kitamura, A.; Hosoda, W.; Sasaki, E.; Mitsudomi, T.; Yatabe, Y. Immunohistochemical Detection of EGFR Mutation Using Mutation-Specific Antibodies in Lung Cancer. *Clin. Cancer Res.* **2010**, *16*, 3349−3355.

(6) Sholl, L. M.; Xiao, Y.; Joshi, V.; Yeap, B. Y.; Cioffredi, L. A.; Jackman, D. M.; Lee, C.; Jänne, P. A.; Lindeman, N. I. EGFR Mutation is A Better Predictor of Response to Tyrosine Kinase Inhibitors in Non-Small Cell Lung Carcinoma Than FISH, CISH, and Immunohistochemistry. *Am. J. Clin. Pathol.* **2010**, *133*, 922−934.

(7) Buttitta, F.; Felicioni, L.; Del Grammastro, M.; Filice, G.; Di Lorito, A.; Malatesta, S.; Viola, P.; Centi, I.; D'Antuono, T.; Zappacosta, R.; Rosini, S.; Cuccurullo, F.; Marchetti, A. Effective Assessment of EGFR Mutation Status in Bronchoalveolar Lavage and Pleural Fluids by Next-Generation Sequencing. *Clin. Cancer Res.* **2013**, *19*, 691−698.

(8) Liu, X.; Lu, Y.; Zhu, G.; Lei, Y.; Zheng, L.; Qin, H.; Tang, C.; Ellison, G.; McCormack, R.; Ji, Q. The Diagnostic Accuracy of Pleural Effusion and Plasma Samples Versus Tumour Tissue for Detection of EGFR Mutation in Patients with Advanced Non-Small Cell Lung Cancer: Comparison of Methodologies. *J. Clin. Pathol.* **2013**, *66*, 1065−1069.

(9) Goto, K.; Ichinose, Y.; Ohe, Y.; Yamamoto, N.; Negoro, S.; Nishio, K.; Itoh, Y.; Jiang, H.; Duffield, E.; McCormack, R.; Saijo, N.; Mok, T.; Fukuoka, M. Epidermal Growth Factor Receptor Mutation Status in Circulating Free DNA in Serum: From IPASS, a Phase III Study of Gefitinib or Carboplatin/Paclitaxel in Non-Small Cell Lung Cancer. *J. Thorac. Oncol.* **2012**, *7*, 115−121.

(10) Goto, K.; Satouchi, M.; Ishii, G.; Nishio, K.; Hagiwara, K.; Mitsudomi, T.; Whiteley, J.; Donald, E.; McCormack, R.; Todo, T. An Evaluation Study of EGFR Mutation Tests Utilized for Non-Small-Cell Lung Cancer in the Diagnostic Setting. *Ann. Oncol.* **2012**, *23*, 2914−2919.

(11) Zong, S.; Wang, Z.; Chen, H.; Yang, J.; Cui, Y. Surface Enhanced Raman Scattering Traceable and Glutathione Responsive Nanocarrier for the Intracellular Drug Delivery. *Anal. Chem.* **2013**, *85*, 2223−2230.

(12) Tian, L.; Gandra, N.; Singamaneni, S. Monitoring Controlled Release of Payload from Gold Nanocages Using Surface Enhanced Raman Scattering. *ACS Nano* **2013**, *7*, 4252−4260.

(13) Qian, X.; Zhou, X.; Nie, S. Surface-Enhanced Raman Nanoparticle Beacons Based on Bioconjugated Gold Nanocrystals and Long Range Plasmonic Coupling. *J. Am. Chem. Soc.* **2008**, *130*, 14934−14935.

(14) Kong, K. V.; Lam, Z.; Goh, W. D.; Leong, W. K.; Olivo, M. Metal Carbonyl−Gold Nanoparticle Conjugates for Live-Cell SERS Imaging. *Angew. Chem., Int. Ed.* **2012**, *51*, 9796−9799.

(15) Qian, X.; Peng, X. H.; Ansari, D. O.; Yin-Goen, Q.; Chen, G. Z.; Shin, D. M.; Yang, L.; Young, A. N.; Wang, M. D.; Nie, S. *In Vivo* Tumor Targeting and Spectroscopic Detection with Surface-Enhanced Raman Nanoparticle Tags. *Nat. Biotechnol.* **2008**, *26*, 83−90.

(16) Wang, X.; Qian, X.; Beitler, J. J.; Chen, Z. G.; Khuri, F. R.; Lewis, M. M.; Shin, H. J.; Nie, S.; Shin, D. M. Detection of Circulating Tumor Cells in Human Peripheral Blood Using Surface-Enhanced Raman Scattering Nanoparticles. *Cancer. Res.* **2011**, *71*, 1526−1532.

(17) Conde, J.; Bao, C.; Cui, D.; Baptista, P. V.; Tian, F. Antibody-Drug Gold Nanoantennas with Raman Spectroscopic Fingerprints for *In Vivo* Tumour Theranostics. *J. Controlled Release* **2014**, *183*, 87−93.

(18) Wang, X.; Yang, D. P.; Huang, P.; Li, M.; Li, C.; Chen, D.; Cui, D. Hierarchically Assembled Au Microspheres and Sea Urchin-like Nanoclusters: Formation Mechanism and SERS Study. *Nanoscale* **2012**, *4*, 7766−7772.

(19) Chen, S.; Huang, P.; Wang, Z.; Wang, Z.; Swierczewska, M.; Niu, G.; Cui, D.; Chen, X. Self-Assembly of Gold Nanoparticles to Silver Microspheres as Highly Efficient 3D SERS Substrates. *Nanoscale. Res. Lett.* **2013**, *8*, 168.

(20) Yang, H.; Deng, M.; Ga, S.; Chen, S.; Kang, L.; Wang, J.; Xin, W.; Zhang, T.; You, Z.; An, Y.; Wang, J.; Cui, D. Capillary-Driven Surface-Enhanced Raman Scattering (SERS)-Based Microfluidic Chip for Abrin Detection. *Nanoscale. Res. Lett.* **2014**, *9*, 138.

(21) Schmidt, M. S.; Hübner, J.; Boisen, A. Large Area Fabrication of Leaning Silicon Nanopillars for Surface Enhanced Raman Spectroscopy. *Adv. Mater.* **2012**, *24*, OP11−OP18.

(22) Goldberg-Oppenheimer, P.; Mahajan, S.; Steiner, U. Hierarchical Electrohydrodynamic Structures for Surface-Enhanced Raman Scattering. *Adv. Mater.* **2012**, *24*, OP175−OP180.

(23) Conde, J.; Baptista, P. V.; Hernández, Y.; Sanz, V.; de la Fuente, J. M. Modification of Plasmid DNA Topology by "Histone-Mimetic" Gold Nanoparticles. *Nanomedicine* **2012**, *7*, 1657−1666.

(24) Wang, L.; Zhang, Z.; Huang, L.; Li, W.; Lu, Q.; Wen, M.; Guo, T.; Fan, J.; Wang, X.; Zhang, X.; Fang, J.; Yan, X.; Ni, Y.; Li, X. Evaluation of Raman Spectroscopy for Diagnosing EGFR Mutation Status in Lung Adenocarcinoma. *Analyst* **2014**, *139*, 455−463.

DOI: 10.1021/am508122e
ACS Appl. Mater. Interfaces 2015, 7, 359−369

(25) Ziegler, C.; Eychmüller, A. Seeded Growth Synthesis of Uniform Gold Nanoparticles with Diameters of 15−300 nm. *J. Phys. Chem. C* **2011**, *115*, 4502−4506.
(26) Wang, L.; He, D.; Zeng, J.; Guan, Z.; Dang, Q.; Wang, X.; Wang, J.; Huang, L.; Cao, P.; Zhang, G.; Hsieh, J.; Fan, J. Raman Spectroscopy: A Potential Tool in Diagnosis and Prognosis of Castration-Resistant Prostate Cancer. *J. Biomed. Opt.* **2013**, *18*, 87001.
(27) Liu, Z.; Yang, Z.; Peng, B.; Cao, C.; Zhang, C.; You, H.; Xiong, Q.; Li, Z.; Fang, J. Highly Sensitive, Uniform, and Reproducible Surface-Enhanced Raman Spectroscopy from Hollow Au-Ag Alloy Nanourchins. *Adv. Mater.* **2014**, *26*, 2431−2419.
(28) Song, J.; Zhou, J.; Duan, H. Self-Assembled Plasmonic Vesicles of SERS-Encoded Amphiphilic Gold Nanoparticles for Cancer Cell Targeting and Traceable Intracellular Drug Delivery. *J. Am. Chem. Soc.* **2012**, *134*, 13458−13469.
(29) Shi, H.; He, X.; Yuan, Y.; Wang, K.; Liu, D. Nanoparticle-Based Biocompatible and Long-Life Marker for Lysosome Labeling and Tracking. *Anal. Chem.* **2010**, *82*, 2213−2220.
(30) Büchner, T.; Drescher, D.; Traub, H.; Schrade, P.; Bachmann, S.; Jakubowski, N.; Kneipp, J. Relating Surface-Enhanced Raman Scattering Signals of Cells to Gold Nanoparticle Aggregation as Determined by LA-ICP-MS Micromapping. *Anal. Bioanal. Chem.* **2014**, *406*, 7003−7014.
(31) Chithrani, B. D.; Ghazani, A. A.; Chan, W. C. Determining the Size and Shape Dependence of Gold Nanoparticle Uptake into Mammalian Cells. *Nano Lett.* **2006**, *6*, 662−668.
(32) Wang, M.; Zheng, L. N.; Wang, B.; Chen, H. Q.; Zhao, Y. L.; Chai, Z. F.; Reid, H. J.; Sharp, B. L.; Feng, W. Y. Quantitative Analysis of Gold Nanoparticles in Single Cells by Laser Ablation Inductively Coupled Plasma−Mass Spectrometry. *Anal. Chem.* **2014**, *86*, 10252−10256.
(33) Zhang, Y.; Chen, B.; He, M.; Yang, B.; Zhang, J.; Hu, B. Immunomagnetic Separation Combined with Inductively Coupled Plasma Mass Spectrometry for The Detection of Tumor Cells Using Gold Nanoparticle Labeling. *Anal. Chem.* **2014**, *86*, 8082−8089.
(34) Yu, J.; Kane, S.; Wu, J.; Benedettini, E.; Li, D.; Reeves, C.; Innocenti, G.; Wetzel, R.; Crosby, K.; Becker, A.; Ferrante, M.; Cheung, W. C.; Hong, X.; Chirieac, L. R.; Sholl, L. M.; Haack, H.; Smith, B. L.; Polakiewicz, R. D.; Tan, Y.; Gu, T. L.; Loda, M.; Zhou, X.; Comb, M. J. Mutation-Specific Antibodies for the Detection of EGFR Mutations in Non-Small-Cell Lung Cancer. *Clin. Cancer Res.* **2009**, *15*, 3023−3028.
(35) Kato, Y.; Peled, N.; Wynes, M. W.; Yoshida, K.; Pardo, M.; Mascaux, C.; Ohira, T.; Tsuboi, M.; Matsubayashi, J.; Nagao, T.; Ikeda, N.; Hirsch, F. R. Novel Epidermal Growth Factor Receptor Mutation-Specific Antibodies for Non-Small-Cell-Lung-Cancer: Immunohistochemistry as a Possible Screening Method for Epidermal Growth Factor Receptor Mutations. *J. Thorac. Oncol.* **2010**, *5*, 1551−1558.
(36) Ellison, G.; Zhu, G.; Moulis, A.; Dearden, S.; Speake, G.; McCormack, R. EGFR Mutation Testing in Lung Cancer: A Review of Available Methods and Their Use for Analysis of Tumor Tissue and Cytology Samples. *J. Clin. Pathol.* **2013**, *66*, 79−89.

DOI: 10.1021/am508122e
ACS Appl. Mater. Interfaces 2015, 7, 359−369